A multicomponent phase-field model for extremely large partition coefficients

Michael J. Welland* and Dieter Wolf
Materials Science Division, Argonne National Laboratory, Argonne, IL 60439, USA.

Jonathan E. Guyer
Materials Science and Engineering Division, Material Measurement Laboratory, National Institute of Standards and Technology, Gaithersburg, Maryland 20899, USA

(Dated: November 25, 2013)

We develop a multi-component phase-field model specially formulated to robustly simulate concentration variations from molar to atomic magnitudes across an interface, i.e.: partition coefficients in excess of $10^{\pm 23}$ such as may be the case with species which are predominant in one phase and insoluble in the other. Substitutional interdiffusion on a normal lattice and concurrent interstitial diffusion are included. The composition in the interface follows the approach of Kim *et al.* [S. G. Kim, W. T. Kim, T. Suzuki, Phys. Rev. E, **60**, 7186 (1999)] and is compared to that of Wheeler *et al.* [A. A. Wheeler, W. J. Boettinger, and G. B. McFadden, Phys. Rev. A. **45**, 7424 (1992)] in the context of large partitioning. The model successfully reproduces analytical solutions for binary diffusion couples and solute trapping for the demonstrated cases of extremely large partitioning.

PACS numbers: 64.70.D-, 81.30.Fb, 05.07.Ln, 66.30.Ny

I. INTRODUCTION

The phase-field method is a popular choice for modeling systems undergoing phase changes due to the versatility of the technique and ready integration with thermodynamic treatments of materials [1–3]. A popular application of the phase-field model is for solidification of pure undercooled melt [4, 5], and binary [6–11] , or multicomponent [12–15] alloys from a liquid, for which the phase-field method can reproduce complex phenomena such as dentritic growth, solute redistribution, and solute trapping.

The phase-field method introduces a new thermodynamic state variable for the system to represent the phase. A two-phase system is thus represented as a single material with the local phase given by a field variable which varies continuously between the two phases, forming a diffuse interface of finite width. Extensive state variables, which in equilibrium may in general be discontinuous across the phase boundary, will likewise vary continuously in phase-field models.

In the case of binary or multicomponent materials, the composition of adjacent phases may vary greatly, resulting in large partition coefficients for individual components. The mole fractions across an interface may vary by several orders of magnitude between phases, as would be the case if one or more components which were abundant, or even dominant in one phase, are "insoluble" in the other. The term insoluble is misleading since it is prohibitively difficult, if not impossible, to completely eliminate any contaminants from a material in practice. There are few phase-field models which consider such large solubility differences [2, 16, 17], despite the fact that it is a common situation. Modeling large solubility variations is a central motivation of this work, in which we develop a model specifically to handle extremely large concentration variations across the interface in a numerically robust, and thermodynamically motivated manner.

Phase-field methods which consider diffusion differ in their treatment of the composition of material in the interfacial region. Some models, including the popular Wheeler, Boettinger and McFadden model, henceforth referred to as WBM, treat interfacial material as a mixture of the two phases at equal composition but differing chemical potential [6, 7, 18, 19]. This results in an extra contribution to the chemical potential in the interfacial region [9] and can be interpreted as a driving force for interfacial adsorption. An alternate approach, and the one which will be assumed in the current work, is to consider the interfacial region as a mixture of the two phases each at their equilibrium compositions with an equal chemical potential [9, 11, 20] referred to as the KKS model after Kim, Kim and Suzuki [9] which has recently been shown to be derivable through a rigorous Lagrangian treatment of the grand canonical potential [15, 21]. This approach ensures that for a stationary interface, the chemical potential is constant throughout the interface [9].

When treating mass transport, one must choose which variable of the species abundance - chemical potential conjugate pair to consider unknown and which to calculate from the thermodynamic model. It is most common to consider species abundance, equivalent to concentration if the volume is constant, and calculate the chemical potential [7, 9]. However, considering the species abundance may result in large variations across the interface while smoothing discontinuities with the phase-field model. An alternative is to consider the chemical potential as the unknown and calculate the concentration from the thermodynamic model [21], since at equilibrium the chemical potential is constant through the interface. In

* mwelland@anl.gov

the current work, we consider the concentration the unknown quantity since the process of inverting the equation of the chemical potential is complicated if the local total concentration of species is not constant, which is the generalization of this work.

Fundamental to phase-field model derivations is the free energy density function and free energy functional. Some functions are constructed as an ideal solution of the pure components [6–8], while others begin with a mechanical mixture of the energies of the two phases and add some excess interfacial energy contributions [3, 9, 20]. The thermodynamic models approach each other when the partition coefficient is approximately 1. In addition, some functionals include gradient energy terms in order to reproduce physical phenomena [7]. The current work assumes a mechanical mixture with excess energy terms, neglecting concentration gradient energy terms since there is little experimental data from which these terms may be obtained, and as will be shown, they are not necessary to produce the range of diffusion phenomena considered in this work.

Consideration of interstitial species diffusing on a separate lattice than the main interdiffusing components is an important step towards modeling the general case of microstructural evolution as it is often encountered in real systems [19, 20]. Since interstitial diffusion does not typically suffer from the numerical pitfalls associated with the main lattice outlined below, it may be treated with more traditional means thus providing a ready comparison between the model developed here and more traditional approaches.

In summary, this work develops a model for isothermal, isobaric, N-species, two-phase systems considering multicomponent diffusion and phase stability in a thermodynamically self-consistent manner. Species diffuse either substitutionally on the main lattice, or on a separate interstitial lattice. The model is derived in a manner which facilitates simulating extremely large solubility gaps. The model is then compared to the classical WBM and KKS models and, under certain special cases, is shown to coincide under first order approximations. Solute trapping is shown to occur at high interface velocities, in accordance with the established theory on the subject [22, 23]. Implementation techniques are discussed in terms of robustness, and an example is shown with abundances varying by a factor in excess of 10^{23} over an interface width of 1 Å, solved numerically using the finite element method with an element size comparable to the interface width, and without artificial stabilization methods or non-physical programming tricks such as boolean statements fixing invalid values.

II. NUMERICAL CONSIDERATIONS

The set of differential equations which will be developed in the following section can only be solved exactly in a limited set of conditions. In general, they must be solved numerically which can lead to issues with numerical robustness and truncation error especially when considering large solubility differences. Such errors may be mitigated by the use of techniques such as the Scharfetter-Gummel discretization scheme [24]. We however choose to take a proactive, preventative stance against these pitfalls and develop our model in such a way as to mathematically *exclude* errors of this nature while still being physically realistic.

There are two cases associated with large variations of constituent concentrations across the phase boundary (large partition coefficients) discussed here. Either case may lead to the numerical method failing to converge on the correct solution or failing entirely due to unreal values being calculated. The mole fraction, upon which configurational diffusion potentials are based, are physically strictly limited to $0 \leq x_i \leq 1$ where $x_i = 0, 1$ relies on the possibility of complete exclusion of a species from a phase. During numerical calculations however, truncation error and the numerical technique can result in mole fraction outside this range, resulting in unreal values being generated or convergence to the wrong solution.

In this approach, we identify the state of the system by the set of species concentrations $\{c_i\}$, with mole fractions x_i, calculated as

$$x_i = \frac{c_i}{\sum_{j=1}^{N} c_j} \tag{1}$$

Furthermore, we consider that in a multicomponent system, no species is ever completely excluded from any phase but rather is vanishingly soluble in which case $c_i > 0$ for all species i, and the mole fractions of all species are limited as $0 < x_i < 1$. The term 'vanishingly' is vague, so we set as a goal mole fractions on the order of 10^{-23} in order to represent an *insoluble* species. Furthermore, we wish to consider systems in which a species is predominant ($x_i \approx 1$) in one phase and *insoluble* in the other, implying partition coefficients on the order of $10^{\pm 23}$.

The combination of extremely small mole fractions and extremely large partition coefficients can produce numerical issues. Truncation error and/or the numerical scheme may produce species concentrations equal to, or less than zero. The associated mole fractions are then less than or equal to zero which can lead to incorrect results or computational failure if the natural logarithms of the mole fractions are being calculated. A simple solution is to treat $lnc_i = \ln(c_i)$ as the quantity of interest rather than c_i. It is a simple matter to recover the concentrations with $c_i = \exp(lnc_i)$, a calculation which can never return a zero or negative result. Additionally, the change of variables makes the algorithm more sensitive to the values of the small concentrations, which might otherwise be rounded off / truncated unless inconveniently high precision variables are used.

Commonly, when solving N interdiffusing species one assumes constant site concentration c_{sites}, and solves

for $N-1$ species, calculating the N^{th} by the equation $c_N = c_{sites} - \sum_{i=1}^{N-1} c_i$. There is no guarantee that, in the course of the numerical procedure, the calculated concentrations and their summation will necessarily be less than c_{sites}, which would imply $c_N < 0$ and can lead to numerical error. We demonstrate that these errors can be *excluded* by calculating the diffusion of all N species independently and using a simple elastomechanics model for internal pressure to enforce the constant site occupancy condition. We can therefore safely assert that $0 < x_i < 1$ *in all cases during the numerical solution scheme* without requiring fine meshes, strict tolerances or unphysical numerical manipulations, allowing the robust use of extremely large concentration variations.

III. MODEL DEVELOPMENT

Derivation of the model begins with the thermodynamic description of the local system, followed by the kinetics of the global system as it evolves. Finally, some material properties, notably the phase-dependent diffusion coefficients, are discussed.

A. Thermodynamic model

In this work we will consider the specific volumes of all species in both phases to be constant. This implies the Gibbs and Helmholtz energies are equivalent, and does not require consideration of bulk movement resulting from changing volume of constituents during diffusion and phase change.

In the following section, square brackets indicate distributive multiplication, round brackets (parenthesis) enclose function arguments, and curly brackets (braces) denote a set of indexed variables. Subscripts $_i$ denote the quantity relates to a particular species, and superscripts $^\alpha$ and $^\beta$ denote the phase. If the subscript or superscript is not included then the quantity is not limited to the associated subset and rather is used in its general context.

In the phase-field method, we introduce a new state variable ϕ which is an order parameter varying continuously in the range $[0,1]$ where $\phi = 0, 1$ represent stable phases α and β respectively. For $\phi = (0,1)$, the material is considered between phases and thus represents an interface. All state variables, including those which exhibit discontinuities such as the species concentrations noted above, will likewise vary smoothly across this interface between their equilibrium values.

We now define two functions related to the phase-field variable. First is the ratio of the local volume of phase β to the total volume, which is calculated by the phase-fraction function $p(\phi) = \frac{V^\beta}{V}$. The form of p is chosen such that $p(\phi = 0, 1) = 0, 1$, and $\frac{\partial p(\phi=0,1)}{\partial \phi} = 0$ which helps place the minima in the energy at the stable phases, $\phi = 0, 1$. A common choice is:

$$p(\phi) = \phi^3 \left[6\phi^2 - 15\phi + 10\right] \tag{2}$$

We also introduce a term which penalizes a system between phases but disappears in the pure phases. A common choice is a parameter W multiplied by a double-well function $K(\phi)$ which is zero in the pure phases:

$$K(\phi) = \phi^2 \left[1 - \phi\right]^2 \tag{3}$$

For the current work, we assume that W is independent of the concentration

If we consider two phases in contact at thermodynamic equilibrium, the equilibrium condition dictates that the thermodynamic potentials (in this case the pressure P and chemical potential of species i $\{\mu_i\}$, are equal, although their conjugate variables volume V, and $\{c_i\}$ may not be. We assume the local free energy density to be a mechanical mixture of the single phase free energy densities at their equilibrium compositions, weighted by the fraction of each phase, and an excess term associated with the excess interfacial energy:

$$g(P, \{c_i\}, \phi) = g^\alpha(P, \{c_i^\alpha\})[1-p] + g^\beta(P, \{c_i^\beta\})p + WK \tag{4}$$

The total concentration of species i is simply the sum of the individual phases weighted by their volume fractions:

$$c_i = c_i^\alpha[1-p] + c_i^\beta p \tag{5}$$

This conception of each phase being at its equilibrium concentration, and therefore having a jump in concentration between phases, is in line with the KKS model [9], as compared with that of WBM [7] which instead assumes both phases are considered at the same concentration which varies smoothly between the equilibrium values.

Let us consider a realistic system of two phases in equilibrium separated by a planar interface. The total Gibbs free energy of this system is proposed to be given by the functional:

$$\boldsymbol{G} = \int_V \left(g(P, \{c_i\}, \phi) + \frac{\epsilon_\phi^2}{2} |\nabla \phi|^2 \right) dV \tag{6a}$$

$$= \int_V \left(g^\alpha[1-p] + g^\beta p + WK + \frac{\epsilon_\phi^2}{2} |\nabla \phi|^2 \right) dV \tag{6b}$$

where ϵ_ϕ is the gradient energy coefficient for the variable ϕ, and is a critical component for the phase-field method. Some models also consider gradient energy terms for the species concentrations, citing that in situations where the diffusion process is of comparable scale to atomic dimensions, gradient energy terms are typically required and include them in their model in order to reproduce solute trapping [7, 8]. Since there is little data from which to obtain coefficients for these terms, they are neglected in

the current model and solute trapping derived in their absence [9].

For a system in equilibrium, the variational derivatives of Eq. (6a) must satisfy:

$$\frac{\delta G}{\delta \phi} = \frac{\partial g}{\partial \phi} - \epsilon_\phi^2 \nabla^2 \phi = 0 \tag{7a}$$

$$\frac{\delta G}{\delta n_i} = \frac{\partial g}{\partial c_i} = \mu_i \tag{7b}$$

where $n_i = c_i V$ is the abundance of species i.

If we consider a system in equilibrium with a planar interface, and label the coordinate normal to that interface $\hat{z}$, Eq. (7a) becomes:

$$0 = \frac{\partial (g^\alpha [1-p] + g^\beta p)}{\partial p} \frac{\partial p}{\partial \phi} + W \frac{\partial K(\phi)}{\partial \phi} - \epsilon_\phi^2 \nabla^2 \phi \tag{8}$$

The first term is the classical lowest common tangent technique for an equilibrium state without consideration of the interface. To see this, we consider that the derivative is being taken while holding the total concentration constant, and therefore must use Eq. (5) to find the rate of change of the concentrations in either phase:

$$\frac{\partial (g^\alpha [1-p] + g^\beta p)}{\partial p} = g^\beta - g^\alpha + \sum_{i=1}^{N} \left(\frac{\partial g^\alpha}{\partial c_i^\alpha} \frac{\partial c_i^\alpha}{\partial p} [1-p] + \frac{\partial g^\beta}{\partial c_i^\beta} \frac{\partial c_i^\beta}{\partial p} p \right) \tag{9a}$$

$$= g^\beta - g^\alpha + \sum_{i=1}^{N} \mu_i \left[c_i^\beta - c_i^\alpha \right] \tag{9b}$$

which is zero in equilibrium with c_i^α and c_i^β assuming their equilibrium values. An exact solution can then be found for the equilibrium phase profile in Eq. (8):

$$\phi(z) = \frac{1}{2} \left[1 + \tanh\left(\frac{z}{2d} \right) \right] \tag{10}$$

where the interface width d, obeys:

$$d = \sqrt{\frac{\epsilon_\phi^2}{2W}} \tag{11}$$

In defining the Gibbs energy density in Eq. (4) we introduced excess energy terms proportional to W and ϵ which disappear in the absence of the interface (i.e.: in the sharp interface). These terms are therefore associated with the interfacial excess energy σ and, if we subtract the bulk free energy of the pure phases from the total Gibbs energy in Eq. (6b) we can assign the interfacial energy directly in our one-dimensional system, with A as the cross-sectional area:

$$\sigma = \frac{1}{A} \int_V \left(W K(\phi) + \frac{\epsilon_\phi^2}{2} |\nabla \phi|^2 \right) dV \tag{12a}$$

$$= \frac{1}{3} \sqrt{\frac{\epsilon_\phi^2 W}{2}} \tag{12b}$$

In the simulation, the interfacial energy is given as a material property and the interface width is a computational parameter. Therefore, we use 11 and 12b to find:

$$\epsilon_\phi^2 = 6\sigma d \tag{13}$$

$$W = 3\frac{\sigma}{d} \tag{14}$$

and the Gibbs energy density and total Gibbs energy can be rewritten:

$$g = g^\alpha [1-p] + g^\beta p + \sigma \frac{3}{d} K \tag{15a}$$

$$G = G^\alpha + G^\beta + \sigma \int_V \left(\frac{3}{d} K + 3d |\nabla \phi|^2 \right) \tag{15b}$$

where $G^{\alpha,\beta}$ are the total Gibbs energies of the α and β phases respectively. Since the Gibbs energy of a heterogeneous system with an interface of area A is $G = G^\alpha + G^\beta + \sigma A$, the term $\left[\frac{3}{d} K(\phi) + 3d |\nabla \phi|^2 \right]$ therefore describes the effective area of the interface smoothed in the direction $\hat{z}$ [25].

1. *Chemical potential*

The Gibbs energy densities in pure phases can be expressed in the integrated form:

$$g^\alpha = \sum_{i=1}^{N} c_i^\alpha \mu_i^\alpha \tag{16}$$

In a pure phase, it is well known that the chemical potential of species i in pure phase α, μ_i^α is given by the equation [25]:

$$\mu_i^\alpha = \mu_i^{0,\alpha} + RT \ln(\gamma_i^\alpha x_i^\alpha) + \int_1^P V_i^* dP \tag{17}$$

where $\mu_i^{0,\alpha}$ is the chemical potential at the standard state and γ_i^α is the activity coefficient which is one for ideal solutions or a function of the state variables in the general case. For this model, we will consider constant pressure P^0, but allow for small variations over which the specific volume of the species (in their pure state) V_i^* is assumed to be constant. Therefore, we define the reference chemical potential $\mu_i^{*,\alpha}(T,P) = \mu_i^{0,\alpha}(T) + \int_1^{P^0} V_i^* dP$ and write:

$$\mu_i^\alpha = \mu_i^{*,\alpha} + RT \ln(\gamma_i^\alpha x_i^\alpha) + V_i^* \Delta P \tag{18}$$

The same expression is true for all species and phases.

The condition of equal chemical potentials of species between phases allows for the definition of the partition coefficient for that species k_i:

$$k_i = \frac{x_i^\alpha}{x_i^\beta} \tag{19a}$$

$$= \frac{\gamma_i^\beta}{\gamma_i^\alpha} \exp\left(\frac{\mu_i^{*,\beta} - \mu_i^{*,\alpha}}{RT} \right) \tag{19b}$$

in which 19b follows Eq. (18). Since this work treats an isothermal situation only, the solubility limits in either phase, and therefore the partition coefficient, do not change.

Since the specific volume of all species are equal in both phases, and the total volume of the system remains constant, we can say $p = \frac{C^\beta}{C}$, and from Eq. (5):

$$x_i = x_i^\alpha[1-p] + x_i^\beta p \tag{20}$$
$$= x_i^\alpha\left[1 - p + \frac{p}{k_i}\right] \tag{21}$$

Substituting this expression into 18 we get an equation for the chemical potential given the total mole fraction, the phase field variable, and the pressure:

$$\mu_i^\alpha = \mu_i^{*,\alpha} + RT\ln\left(\gamma_i^\alpha \frac{x_i}{1-p+p/k_i}\right) + V_i^*\Delta P \tag{22a}$$
$$\mu_i = \mu_i^{*,\alpha} + RT\ln(\gamma_i^\alpha x_i) - RT\ln(1-p+p/k_i) + V_i^*\Delta P \tag{22b}$$

where we have dropped the superscript since the chemical potential in both phases is equal.

It is noted here that if μ_i is constant over the domain and all sites are occupied, $\Delta P = 0$ and Eq. (22b) gives a simple and intuitive mole fraction profile in terms of the phase-fraction:

$$x_i = x_i^\alpha + p\left[x_i^\beta - x_i^\alpha\right] \tag{23}$$

where the activity coefficient γ_i^α has dropped out since it is a function of the state variables in the α phase only, which are constant through the interface. Equation 23 is equivalent to 20 but valid over the whole domain, whereas the latter is defined locally.

The excess interfacial term W is not introduced in Eq. (23) since it is independent of the concentration. If we did have a concentration dependence, such as $W = \sum_{i=1}^{N} c_i W_i$ then the chemical potential would be:

$$\mu_i = \mu_i^{*,\alpha} + RT\ln(\gamma_i^\alpha x_i) - RT\ln(1-p+p/k_i) + V_i^*\Delta P + W_i K \tag{24}$$

It is sometimes desirable to show how the free energy function of a solution relates to that of the pure phases. From Eq. (24) we get:

$$\mu_i = \mu_i^{*,\alpha} + RT\ln(\gamma_i^\alpha x_i) + pRT\ln\left(\frac{\gamma_i^\alpha}{\gamma_i^\beta}k_i\right) - RT\ln\left(\left[1-p+\frac{p}{k_i}\right]\left(\frac{\gamma_i^\alpha}{\gamma_i^\beta}k_i\right)^p\right) + V_i^*\Delta P + W_i K \tag{25a}$$
$$= g_i(P,p) + RT\ln(\gamma_i^\alpha x_i) - RT\ln\left(\left[1-p+\frac{p}{k_i}\right]\left(\frac{\gamma_i^\alpha}{\gamma_i^\beta}k_i\right)^p\right) \tag{25b}$$

where we have used 19b, and identified the single component, two-phase molar Gibbs energy:

$$g_i(P,p) = \mu_i^{*,\alpha} + p[\mu_i^{*,\beta} - \mu_i^{*,\alpha}] + V_i^*\Delta P + W_i K \tag{26}$$

B. Kinetics

We now have a thermodynamic model of a macroscopic system exhibiting gradients in the state parameters. The temporal evolution of the system can be derived through the theory of irreversible processes, which essentially guarantees that local processes, such as mass transport and phase change, must produce entropy [26, 27]. Since we are under conditions of constant temperature and pressure, this implies the monotonic decrease of the system's Gibbs energy.

In writing the following equations, we consider a system with a single interstitial species, denoted by subscript $_I$, diffusing on a separate lattice. As an approximation, the interstitial will be assumed to fit entirely in free space in the main lattice and therefore have zero partial molar volume. As a simple model, we consider the concentration of interstitial sites to be a fixed multiple of the concentration of substitutional species, which does not deviate much from the equilibrium density. In fact, the concentration of interstitial sites may depend on a number of factors. In order to keep the total interstitial site concentration constant, we consider interstitial diffusion to be the interdiffusion of occupied and unoccupied sites. Since we consider only the case where the interstitial sites are mostly unoccupied, we can use the typical approach of assuming a constant total concentration and calculating the concentration of unoccupied interstitial sites from this condition without fear of the numerical difficulties outlined previously in the context of substitutional species.

The local pressure, which varies only slightly from the atmospheric pressure, is treated quasistatically:

$$\frac{1}{\kappa} = -\frac{1}{V}\frac{\partial V}{\partial P} \tag{27a}$$
$$\Delta P = -\kappa\ln\left(\frac{V(P)}{V(P^0)}\right) \tag{27b}$$

where κ is the isothermal bulk modulus. If we defined the normal site concentration c_{sites} as being held constant, then the current volume is also fixed: $V(P) = c_{sites}V_i^*$. If no internal pressure were present, the volume would be dictated by the number of chemical species $V(P^0) = V_i^*\sum_{i=1}^{N} c_i$. Therefore, the local pressure differential is:

$$\Delta P = -\kappa\ln\left(\frac{c_{sites}}{\sum_{i=1}^{N} c_i}\right) \tag{28}$$

such that if the local total species concentration diverges from the equilibrium concentration, a local pressure is generated which drives mass flux via the chemical potential in Eq. (24) to restore the normal concentration. This approach is physically realistic, and enables the tracking of the N interdiffusing species independently, thus allowing increased numerical robustness as discussed in Section 2.

The phase-field evolution equation is:

$$\frac{\partial \phi}{\partial t} = -M_\phi \frac{\delta \boldsymbol{G}}{\delta \phi} - \nabla \cdot (\vec{v}\phi) \tag{29a}$$

$$= -M_\phi \left[\frac{\partial g}{\partial \phi} - \epsilon_\phi^2 \nabla^2 \phi \right] - \nabla \cdot (\vec{v}\phi) \tag{29b}$$

$$= -M_\phi \left[\sum_{i=1}^{N} c_i \frac{\partial \mu_i}{\partial \phi} - \epsilon_\phi^2 \nabla^2 \phi \right] - \nabla \cdot (\vec{v}\phi) \tag{29c}$$

where M_ϕ is the kinetic coefficient which can be considered related to the attachment kinetics term in solidification and $\vec{v}$ is the velocity of the frame of reference.

The rate of change in the local abundance of species i is given by the conservation equation:

$$\frac{\partial c_i}{\partial t} = -\nabla \cdot \left(\vec{J}_i + c_i \vec{v} \right) \tag{30}$$

with the diffusive flux of species i $\vec{J}_i$, being proportional to the variation of the Gibbs energy with the concentration:

$$\vec{J}_i = -c_i M_i \nabla \frac{\delta \boldsymbol{G}}{\delta n_i} \tag{31}$$

where M_i is the mobility of species i.

For substitutional species, the concentration of each species varies independently and $\frac{\delta \boldsymbol{G}}{\delta n_i} = \mu_i$. For the interstitial species, the constraint of constant interstitial lattice sites implies that diffusion of the interstitial species coincides with a counter diffusion of unoccupied interstitial sites, and therefore that $\frac{\delta \boldsymbol{G}}{\delta n_I} = \mu_I - \mu_{unoccupied}$. The flux equation therefore become:

$$J_i = \begin{cases} -c_i M_i \nabla \mu_i & \text{main lattice species} \\ -c_I M_I \nabla \left(\mu_I - \mu_{unoccupied} \right) & \text{interstitial species} \end{cases} \tag{32}$$

Since in the current model, each point in the interface is at thermodynamic equilibrium, we can use the Gibbs-Duhem equation to simplify the interstitial case:

$$J_i = \begin{cases} -c_i M_i \nabla \mu_i & \text{main lattice species} \\ -c_I \frac{1}{1-x_I} M_I \nabla \mu_I & \text{interstitial species} \end{cases} \tag{33}$$

The mobility is readily related to the diffusion coefficient by comparing with Fick's law: $J_i = c D_i \nabla x_i$. The gradient of the chemical potential in a single phase is given by 17:

$$\nabla \mu_i = \frac{RT}{x_i} F(x_i) \nabla x_i \tag{34}$$

where $F(x_i) = \left[1 + \frac{\partial \ln \gamma_i}{\partial \ln x_i} \right]$ is the thermodynamic factor. The mobilities are therefore:

$$M_i = \begin{cases} \frac{D_i}{RT} \frac{1}{F_i} & \text{main lattice species} \\ (1 - x_I) \frac{D_I}{RT} \frac{1}{F_I} & \text{interstitial species} \end{cases} \tag{35}$$

and so the flux equations become:

$$J_i = -c_i \frac{D_i}{RTF_i} \nabla \mu_i \tag{36}$$

Valid for both substitutional and interstitial species i.

C. Material properties

Since we are not concerned with elastomechanic effects in the current work, a realistic constant value of the isothermal bulk modulus κ in Eq. (28), typically on the order of gigapascals, is sufficent to ensure approximately constant site fraction occupancy.

Since the current work is not concerned with attachment kinetics, a large value of M_ϕ is taken in order to assure local equilibrium. Alternately, one can consider the phase stability fast enough to always be in equilibrium, in which case Eq. (29b) is quasistatic and we can remove M_ϕ entirely. In the authors' experience the quasistatic approach, while attractive in simplicity and reassuring in the desired local equilibrium generally leads to less stability in the resulting equations.

In the sharp interface model, mass diffusion occurs in both phases (at different compositions) independently while being coupled at the interface. In order to determine the diffusion coefficient for use in the current phase-field model we must consider that the net mass transport from diffusion in two separate phases is being represented by diffusion in a single material parameterized by the phase fraction function p, in addition to the fact we are representing two concentrations c_i^α and c_i^β, with a single variable c_i.

If one considers that the total mass flux in a two-phase region be equal to the sum of the mass fluxes in both phases at their respective compositions, then we find:

$$J_i = -c^\alpha D_i^\alpha \nabla x_i^\alpha - c^\beta D_i^\beta \nabla x_i^\beta \tag{37a}$$

$$= -c \left[D_i^\alpha [1-p] + D_i^\beta \frac{p}{k_i} \right] \nabla x_i^\alpha \tag{37b}$$

where c is the total concentration of all species in both phases, and we have assumed that the location and orientation of the interface does not interfere with the flux of mass through the element, an assumption inherent in the phase-field method.

We can now compare Eq. (37b) with Eq. (36), and use Eq. (18) assuming an equilibrium $\Delta P = 0$:

$$-c \left[D_i^\alpha [1-p] + D_i^\beta \frac{p}{k_i} \right] \nabla x_i^\alpha = -c_i \frac{D_i}{RT} RT \frac{1}{x_i^\alpha} \nabla x_i^\alpha \tag{38}$$

$$D_i = \frac{c}{c_i} x_i^\alpha \left[D_i^\alpha [1-p] + D_i^\beta \frac{p}{k_i} \right] \tag{39a}$$

$$= \frac{D_i^\alpha [1-p] + D_i^\beta \frac{p}{k_i}}{1 - p + \frac{p}{k_i}} \tag{39b}$$

where we have used Eq. (21). The total diffusion coefficient in Eq. (36) is therefore the sum of the diffusion coefficients in either phase weighted by both the phase fraction and the partition coefficient. Note that for $\phi = 0, 1$, $D_i = D_i^\alpha, D_i^\beta$ respectively and that if the phase change occurs congruently, $k_i = 1$ and the diffusion coefficient is simply weighted by the phase fraction.

IV. SIMULATION RESULTS AND DISCUSSION

The system of equations described above were implemented and solved using the open source finite element package FEniCS [28–32]. All variables were represented with linear Lagrange elements. Newton's method was used to solve the non-linear system of PDEs with absolute and relative tolerances set to 10^{-10} and 10^{-10} respectively, and consistently exhibited quadratic convergence. Adaptive time stepping is done with the aid of the Gryphon module, and uses a singly implicit Runge-Kutta method with an explicit first stage with absolute and relative tolerances set to 10^{-3} and 10^{-4} respectively unless otherwise noted [33, 34]. Element size for the simulations were set as $\frac{d}{10}$ in order to obtain high resolution curves, however the authors note that the model converges with element sizes of $\frac{d}{2}$ to reasonable results but with errors as one would expect from poorly defined elements. The thermodynamic solutions are treated as ideal, in which case all activity coefficients are equal to unity. A selection of codes are available on the author's personal website [35].

In order to reach very large partitioning, it was found helpful to introduce a helper variable $\phi_2 = 1 - \phi$ and calculate $p_2(\phi_2) = p(\phi_2) = 1 - p(\phi)$ in the same manner as Eq. (2). The chemical potential in Eq. (22b) is then implemented as:

$$\mu_i = \mu_i^{*,\alpha} + RT \ln(\gamma_i^\alpha x_i) - RT \ln(p_2 + p/k_i) + V_i^* \Delta P \tag{40a}$$

The use of this variable helps prevent roundoff errors when $\phi \approx 1$.

We therefore calculate the following variables locally at each point: the total concentration of each species considering all phases locally present, the pressure, and the phase-field variable and its helper.

Simulation results are divided into sections of increasing complexity, and demonstrate the ability and implications of extremely large partition coefficients. First, a comparison between the current model and a different consideration of compositions in the interface is shown. Second, the proposed model is compared quantitatively in terms of performance with the 'classic' WBM and KKS models. Third, the simulation is applied to a binary diffusion couple with both the normal lattice diffusion model and the interstitial diffusion model and compared with the exact solution for cases of the same and different diffusion coefficients. Fourth, the reproduction of solute trapping effects is demonstrated which, although not the focus of the current work, demonstrates the versatility of the model. Finally the potential of the model is demonstrated with a two-phase quinary system with four interdiffusing species and one lattice species, which vary from abundant to insoluble in either phase.

A. Comparison to other models

In the current model, we consider the equality of the chemical potentials in the interfacial, two-phase region, with the consequence that the compositions in coexisting phases may not be equal. This approach is the same as that taken by Kim *et al.* [9] and since cited numerous times [3, 12, 13, 19, 20, 36]. An alternative model for alloy solidification was proposed by Wheeler *et al.* [6, 7] which considers the chemical compositions to be equal in the interfacial region and only shows the equilibrium solubility gap far from the interface. As commented by Kim *et al.*, this implies the chemical potential is not flat across the interface but has an extra contribution [9]. This also places limits on the size of the interface, and makes certain material properties vary depending on the interface thickness [10]. As we will show here, it also results in composition profiles that are not simple interpolations between the bulk phases, notably in multicomponent cases, when the partition coefficient of a species is outside the range $1/2 < k_i < 2$.

We can explore this model by setting $c_i^\alpha = c_i^\beta = c_i$ in Eq. (4) followed by Eq. (16). In order to distinguish between the previous model and this one, functions corresponding to this interpretation will be written with a tilde.

$$\widetilde{g} = g^\alpha(P, \{c_i\})[1-p] + g^\beta(P, \{c_i\})p + WK \tag{41a}$$

$$= \sum_{i=1}^{N} c_i [1-p] \mu_i^\alpha(P, \{c_i\}) + c_i p \mu_i^\beta(P, \{c_i\}) + c_i W_i K \tag{41b}$$

$$= \sum_{i=1}^{N} c_i \widetilde{\mu}_i \tag{41c}$$

where the total chemical potential of species i in the two phase system can be derived with the help of Eq. (18) and Eq. (19b):

$$\widetilde{\mu}_i = [1-p]\mu_i^\alpha(P, \{c_i\}) + p\mu_i^\beta(P, \{c_i\}) + W_i K \tag{42a}$$

$$= \mu^{*,\alpha} + pRT \ln(k_i) + RT \ln(\gamma_i^\alpha x_i) + V_i^* \Delta P + W_i K \tag{42b}$$

$$= g_i(P, \phi) + RT \ln(\gamma_i^\alpha x_i) \tag{42c}$$

where we have used Eq. (26).

In comparing the definition of chemical potential between Eq. (42c) and 25b, we see a different functional dependence on the phase fraction p, although the expressions are equal when $p = 0, 1$ as expected. The difference only manifests when the interfacial region is considered. The right most term in 25b is the origin of the discrepancies between the conceptions and contributes the extra free energy noted by Kim [9]. It is noted however, that the two equations are reconcilable in the special case when k_i is not far from unity. In this case, the last term in 25b can be expanded about the point $k = 1$:

$$\ln\left(\left[1-p+\frac{p}{k_i}\right]\left(\frac{\gamma_i^\alpha}{\gamma_i^\beta}k_i\right)^p\right) \approx p\ln\left(\frac{\gamma_i^\alpha}{\gamma_i^\beta}\right)+\mathcal{O}\left((k-1)^2\right) \tag{43}$$

which converges if $|1 - k_i| < 1$. If we make the common assumption of an ideal solution, then to a first order approximation in $(k-1)$ this term may be neglected. However for partition coefficients greater than this, the series expansions diverge and the approximation is no longer a good one.

The inclusion of an excess chemical potential term, which is confined to the interface, effectively introduces interfacial adsorption, the degree of which depends on the partition coefficient. Let us consider a steady state case of an ideal solution without center of mass movement, and that the internal pressure differential is everywhere zero. In equilibrium, all mass fluxes should be zero. We impose zero pressure differential and can therefore solve for $N - 1$ species, the N^{th} being determined by $\sum_{i=1}^{N} c_i = c_{sites}$, where each mass flux is given by $J_i \propto \nabla(\mu_i - \mu_N) = 0$. Since W_i is constant for all species, the term $W_i K$ cancels from the expressions for the chemical potentials.

With the current model, the solution is trivial and given by 23:

$$x_i = x_i^\alpha + p\left[x_i^\beta - x_i^\alpha\right] \tag{44}$$

such that $\nabla\mu_i = 0$ for all species. This can be considered equivalent to the sharp interface model with the interface smoothed between the end compositions.

In the case of Eq. (42b), the general solution is no longer so easily obtained since the phase fraction is not enclosed in a logarithm as is the mole fraction. Considering each $\nabla\tilde{\mu}_i = 0$ results in a mole fraction profile interpolated geometrically between the equilibrium values:

$$\tilde{x}_i = [x_i^\alpha]^{1-p}\left[x_i^\beta\right]^p \tag{45}$$

which cannot be true for all species since, for example in the binary system case:

$$1 - \tilde{x}_i \neq [1 - x_i^\alpha]^{1-p}\left[1 - x_i^\beta\right]^p \tag{46}$$

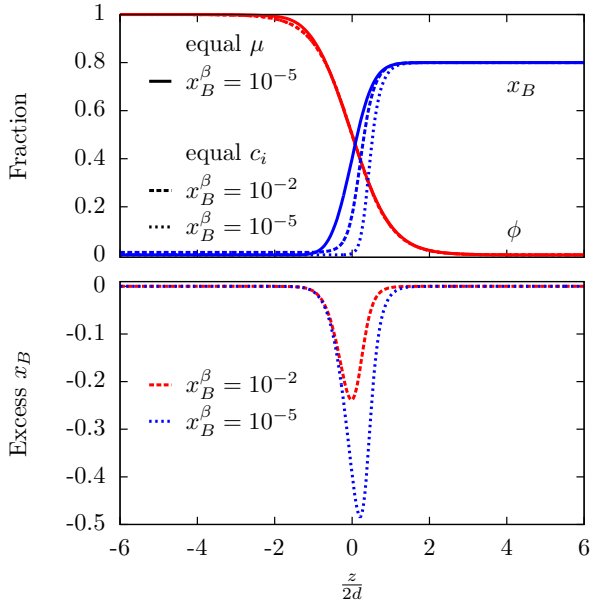

FIG. 1. Simulation results for a binary, two-phase material using the current model based on constant chemical potential in the interface, and constant mole fraction from reference [6]. A series of plots with different boundary values of x_B^β are plotted, showing the effect on the resulting composition profile and phase-field.

In general, the equilibrium for these models must be solved numerically, as is shown in Figure 1 for $k_B = 80$ and 80 000 as a function of the dimensionless distance coordinate $\frac{z}{2d}$ from Eq. (10). The difference between the current model and that described above may be viewed as the interfacial adsorption is also shown in the bottom of the figure. Of note is the effect of apparently *narrowing* of the interface width, as seen in the concentration profile, while the phase field profile is not greatly affected. The concentration profile becomes sharper with larger partition coefficients.

The quantity of adsorbed species depends on the differences between the terms in Eq. (43), which in turn depends on the partition coefficients. Figure 1 reveals that this dependence on the partition coefficient increases with the severity of the partitioning and is not symmetric about the point $\phi = 0.5$ on a linear ordinate scale as one may intuit, although it is noted that it is symmetric about this point on a logarithmic scale.

An example of a ternary simulation result is shown in Figure 2 with equilibrium mole fraction vectors $x^\alpha = (.4, .05, .55)$ and $x_i^\beta = (.01, .6, .39)$ along with the differences between curves.

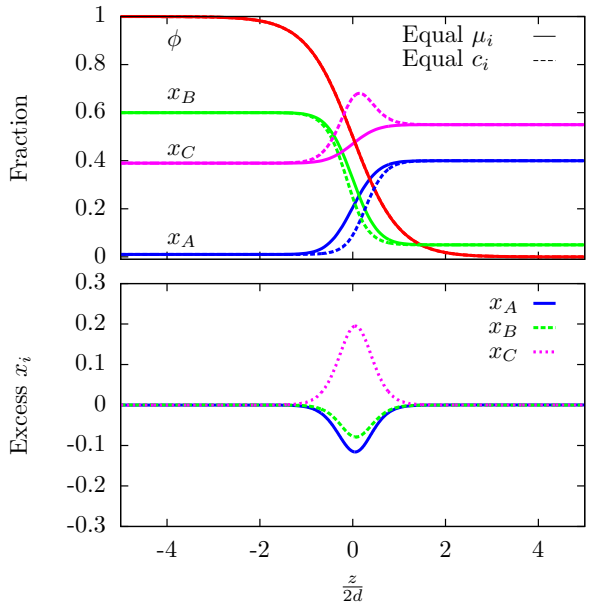

FIG. 2. Simulation results for a ternary, two-phase material using the current model based on constant chemical potential, and that with constant mole fraction. The difference between the curves, representative of interfacial adsorption is shown below.

TABLE I. Material properties for a transient binary two phase simulation, used for a performance comparison.

D_i^α[µm^2 s^{-1}]	D_i^β[µm^2 s^{-1}]	$x_B^{\alpha,eq}$	M_ϕ	d[Å]
1.0	1.0	0.1	10^2	1.0

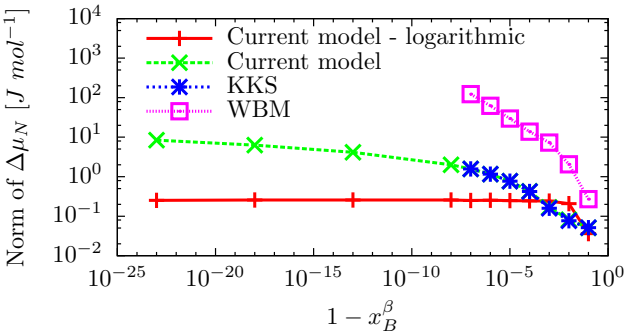

FIG. 3. Comparison between steady state solutions of binary diffusion problems with x_B^β approaching unity. Values shown are the norm of the error in the N^{th} component which is not calculated explicitly in the classical KKS and WBM models. The classical models' data terminates where non-real values are encountered.

B. Performance comparison

It is useful to quantify the performance of the current model compared to the classical KKS and WBM models without the above described modifications. Since numerical robustness and sensitivity to small quantities were the motivations of this work, performance may suffer in exchange. Indeed, this can be expected intuitively since more variables have been introduced into the problem, thus making the system larger and more nonlinear.

We compare four models: the WBM and KKS models calculating only one concentration and without using the logarithmic transformation, and the model proposed in this work with and without the logarithmic transformation of the concentration variables. In order to fairly compare the performance of the WBM model and the KKS-based ones, we must consider that the steady state solution for the WBM model is non-trivial as discussed above. Indeed, the behavior of Newton's method in solving stationary problems would be a practical standard to use to investigate the robustness of the model but since the convergence of this method is largely related to the quality of the initial guess, such an examination would be biased to the KKS-based models. To obtain steady state solutions for the WBM model, or fair initial conditions, we therefore resort to a transient simulation with a long run time to obtain steady state solutions.

We first consider the ability of the models to resolve small concentrations and their corresponding chemical potentials in a steady state situation. A binary, two-phase system is simulated in which the composition is fixed in one phase, $x_B^\alpha = 0.1$ and the composition at the other boundary approaches 1: $x_B^\beta \to 1$. Material properties are given in Table I. For the KKS and WBM models, only c_B is calculated. In the steady state, the interdiffusion potential, $\mu_B - \mu_A$ should be constant and calculable from the boundary conditions, thus providing a means to check the error of the calculation. The norm of this error is plotted against the departure from unity in Figure 3 for the four models.

The data for the classical KKS and WBM models terminate at $1 - x_B^\beta = 10^{-7}$, past which roundoff prohibited calculation of the chemical potential. The location of this point depends on system architecture, variable precision and even programming technique. It is of course the precise motivation of the current work to avoid such errors, which is demonstrated in the figure where the current model allows values to be calculated all the way down to atomic concentrations of species A in the β phase.

The current model without the logarithmic transformation matches the KKS results very well where the latter converged. All models lose accuracy as $x_B^\beta \to 1$, however it is clear that the logarithmic transformation succeeds in maintaining accuracy in concentrations and the chemical potentials.

To compare the performance of the models, a simple transient scenario was implemented with an adaptive time stepping algorithm, the behavior of which provided practical quantitative data. The accuracy of the simu-

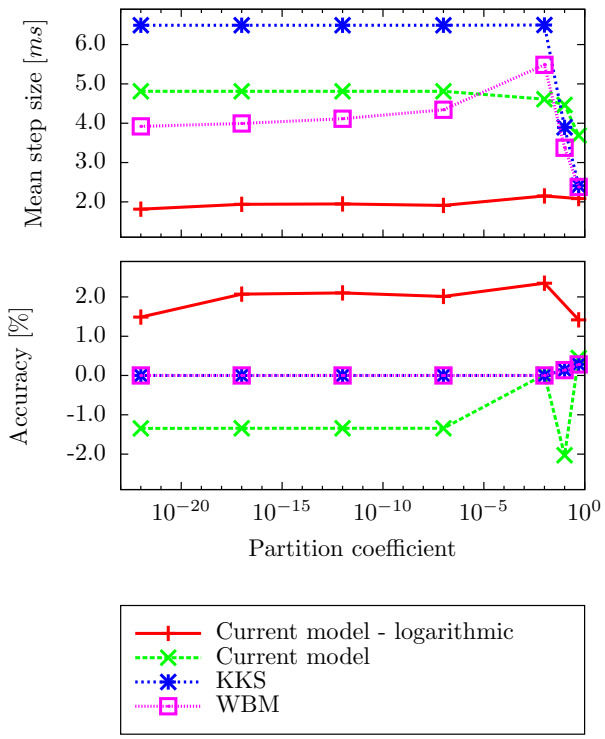

FIG. 4. Performance comparison between the WBM and KKS models implemented without the logarithmic transformation outlined in this article, and the current work with and without the transformation. The average step size chosen by the adaptive time stepping algorithm is shown above, and the accuracy of the model compared to the exact solution is shown below.

lation can be calculated by comparison with the exact solution.

A two phase binary solution was simulated with a constant inward flux of $1 \times 10^{-2}\,\mathrm{mol\,m^{-2}\,s^{-1}}$ to the α phase. The value of c_B^β was varied in order to implement different partition coefficients. The same material properties in Table I are used. The initial conditions for the transients were steady state solutions as described above. A simulation time of 1 s was then simulated, starting with an initial time step of 1×10^{-7} s. The exact increase in integrated concentration is therefore 1×10^{-2} mol.

Statistical reports generated from the Gryphon module were collected and are used to quantify the performance / behavior of the models as shown in Figure 4. The top and bottom graphs show the average step size taken by the adaptive time solver, and the percent difference between the simulated and exact concentration increment respectively. Average variance in step size was less than one percent. All the models took 20 residual evaluations per step on average.

In terms of step size, the WBM model increased its step size as the partition coefficient approached 1 whereas the other models, all KKS based, remained approximately constant. An explanation for the behavior of the WBM model may be that the interface effectively shrinks when the partition coefficient is far from 1, which implies more rapidly varying variables and therefore a smaller time step. At $k = 10^{-3}$, the WBM model exceeds the equivalent KKS model's time step, possibly due to the increased mathematical complexity of the latter. It is reassuring that the KKS and WBM models meet when $k = 0.5$ as predicted by the discussion above.

The rather sharp decrease in step sizes for all of the models at the right of the graph may be due to c_B^β becoming of significant magnitude and therefore contributing more to the time derivative. There is no decrease in step size for the current model with the logarithmic representation since the logarithm of concentration does not vary as strongly due to the nature of the transformation.

In terms of accuracy, the current model suffers with and without the logarithmic transformation compared to the 'classical' KKS and WBM models for the same tolerance on the time stepping. Higher accuracy can be obtained with smaller time steps. The reason for this may be the ability of the model to have slightly higher or lower local densities, if the elastic stresses are not exactly zero. This flexibility is however important to allow for large concentration variations with numerical robustness.

Interestingly, the accuracies of all the models change slightly for smaller partitioning, the cause of which is not immediately clear.

C. Comparison to exact solution

Analytical solutions to problems of binary interdiffusion and moving boundaries are well known in terms of error functions and constitute a good test of this model. We will consider the situation of two initially pure materials of different elements joined at time $t = 0$. The two elements form a solubility gap on either side of the interface, which moves with time. Elements are supposed to interdiffuse through direct exchange, which eliminates the Kirkendall effect from the current analysis for the sake of simplicity. The analytical solution for the concentration profiles is:

$$x_i = \begin{cases} \frac{C^{\alpha,e}}{\mathrm{erfc}(-\lambda\sqrt{\psi})}\,\mathrm{erfc}\left(\frac{-x}{2\sqrt{D^\beta t}}\sqrt{\psi}\right) & \text{for } -\infty < x < \epsilon(t), \\ 1 + \frac{C^{\beta,e}-1}{\mathrm{erfc}(\lambda)}\,\mathrm{erfc}\left(\frac{x}{2\sqrt{D^\beta t)}}\right. & \text{for } \epsilon(t) < x < \infty \end{cases} \tag{47}$$

where $\psi = \frac{D^\beta}{D^\alpha}$ and the interface postition is given by:

$$\epsilon(t) = 2\lambda\sqrt{D^\beta t} \tag{48}$$

The value of λ must be determined numerically by solving the trancedental equation:

$$(c^{\beta,e}-1)\frac{e^{-\lambda^2}}{\mathrm{erfc}(-\lambda)} + c^{\alpha,e}\frac{e^{-\lambda^2\psi}}{\sqrt{\psi}\,\mathrm{erfc}(\lambda\sqrt{\psi})} = (c^{\beta,e}-c^{\alpha,e})\lambda\sqrt{\pi} \tag{49}$$

TABLE II. Material properties for binary diffusion couple simulations and the exact solutions. Since a direct interchange diffusion model is assumed, the diffusion coefficients of each species are equal.

	D_i^α[μm^2 s^{-1}]	D_i^β[μm^2 s^{-1}]	$x_B^{\alpha,eq}$	$x_B^{\beta,eq}$	M_ϕ	d_ϕ[Å]
Trial #1	1	1	0.7	0.15	10^{10}	1
Trial #2	1	10^{-5}	0.7	0.15	10^{10}	1

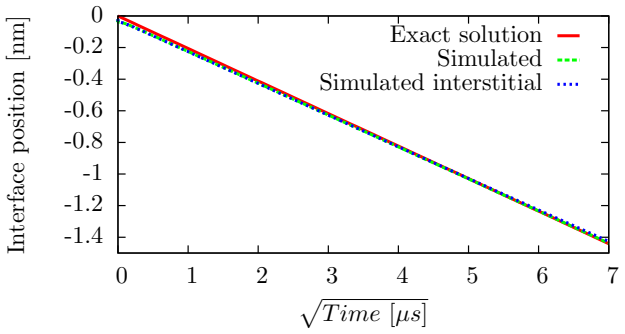

FIG. 5. Simulation results for normal lattice model and interstitial model compared against exact results with $\lambda = -0.1029$.

In the phase-field model, we take 'joining' to imply the formation of a continuous material varying between phases (pure components), permitting interdiffusion to take place. The initial condition for the phase-field variable is the exact solution from Eq. (10), and the concentration profiles following the corresponding $p(\phi)$ profile. The interface is therefore not in equilibrium with respect to the interdiffusing species and experiences an initial transient and slight shift in position as the solubility limits are established before reaching the normal behaviour described by the exact solution.

Figure 5 shows a comparison of the interface position determined from the exact solution, interdiffusion between main lattice species, and the diffusion of an interstitial species as a point of comparison. Material properties and the parameters of the exact solution are given in Table II. Intitial conditions for the simulated concentration profiles are $x_i = 1 - 10^{-23}$ in the "pure" material and $x_i = 10^{-23}$ in the phase in which it is "insoluble". The simulation results are shifted by a fit parameter 3.5×10^{-2} nm, which accounts for the interfacial movement during the initial transient. The location of the interface in the phase-field models is the contour of $\phi = 0.5$. The initial transient is clearly observed before the exact solution behavior is reached. Excellent agreement is then observed between the two lattice diffusion models and the exact solution.

The application of the phase-field method in smoothing discontinuous functions can be seen by comparing the simulated concentration profiles with the predictions of the exact solution. This is shown for species B in Figure 6.

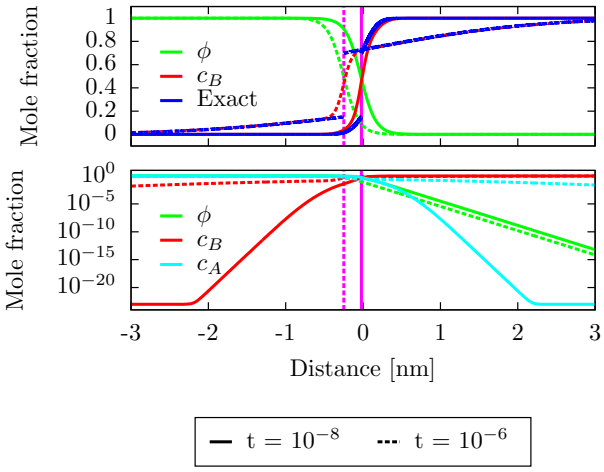

FIG. 6. Calculated profiles compared with exact solutions for times 10^{-8}, 10^{-6} with $D^\alpha = D^\beta = 10^{-12}$ on linear and logarithmic scales (above and below respectively). The current exact interface position is indicated by vertical lines.

The results of simulations with phase dependent diffusion coefficients is shown in Figure 7 with a few concentration profiles shown in Figure 8. Material properties and exact solution parameters are given in Table II. Excellent agreement is noted in the comparison between interface position predicted by the exact solution and simulation. Figure 8 shows good agreement for the concentration profiles although for $t = 10^{-5}$, the concentration profile in the α phase does not follow the exact solution very well.

The cause of the odd behavior in the concentration profile in the α phase is a superposition of two effects caused by the interface width being of comparable magnitude to the diffusion length in that phase. The smooth variation between $c_B = .15$ and $c_B = .7$ is maintained by the concentration discontinuity being smoothed over the phase-field interpolation function p, which already accounts for the horizontal distance between the exact and simulated predictions. Having understood this, one may still expect a very sharp gradient after the interface is complete, between $c_B = 0.7 \to 1.0$, comparable to the steepness of the exact solution and a consequence of the small diffusion coefficient. The reason this slope is smooth is that ϕ remains greater than zero albeit by a very small amount, as evident by the logarithmic plot below. Through the expression for the diffusion coefficient in 39b then, the simulated diffusion coefficient is not yet D_i^α, but still incorporates a small fraction of the much larger D_i^β. This could be viewed as a limitation,although not necessarily an error, of the current phase-field model as compared to the sharp-interface case, although the agreement between predicted interface positions should not be forgotten despite this complication.

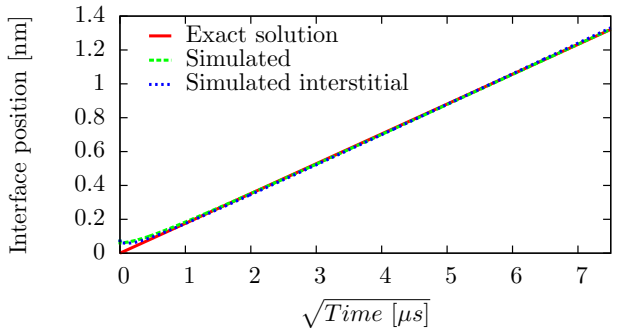

FIG. 7. Simulation results for normal lattice model and interstitial model compared against exact results with $\lambda = 0.0881$.

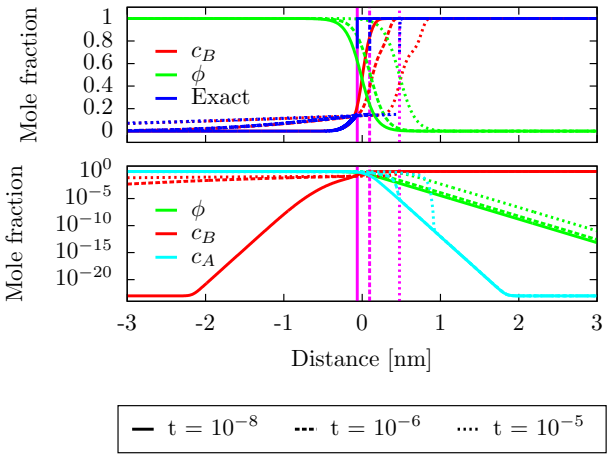

FIG. 8. Calculated profiles compared with exact solutions for times 10^{-8}, 10^{-6} 10^{-5} with $D^{\alpha} = 10^{-12}$ and $D^{\beta} = 10^{-17}$. Linear and logarithmic scales are shown above and below respectively. The current exact interface position is indicated by vertical lines.

D. Solute trapping

In the case of sufficiently high interface velocities, such as might be the case of a supercooled liquid, the interface may propagate faster than diffusion of species ahead of the interface may be able to reestablish local equilibrium. This leads to the phenomenon of solute trapping in which a chemical potential jump exists across the interface. The magnitude of the chemical potential jump depends on the interface propagation speed, leading to a ratio of mole fractions on either side of the interface to be quite different from the equilibrium partition coefficient. The phenomenon has been modeled previously using the phase-field method in which case the jump in chemical potential is smoothed between pure phases [6, 7, 9, 19, 20, 23]. As pointed out by Kim *et al*, the gradient of chemical potential across the interface does not contradict the assumption of local equilibrium between chemical potentials, and therefore does not exclude this phenomenon [9].

TABLE III. Material properties for the solute trapping simulations

D_i^{α}[μm^2 s^{-1}]	D_i^{β}[μm^2 s^{-1}]	$x_A^{\alpha,eq}$	$x_A^{\beta,eq}$	M_{ϕ}	d_{ϕ}[Å]
1	1	10^{-13}	1^{-23}	10^{10}	1

The consequence of trapping is the shifting of the solid composition towards that of the liquid, and a pile-up of solute on the liquid side. At high speeds, the solid concentration becomes equal to that of the liquid *far from the interface* while the liquid at the interface is driven far from its equilibrium value by the attempt to keep the equilibrium partition coefficient, leading to a pile-up of the species. At very high speeds, the equilibrium partitioning force is overcome and the pile-up disappears leaving the ratio of concentrations in the liquid and solid the same.

One can describe this phenomenon in a sharp interface model with an effective partition coefficient k^* which is the velocity dependent ratio of the solid concentration at the interface to that of the liquid [22, 23]. The model of Ahmad *et al.* yields an expression (in our nomenclature):

$$\ln\left(\frac{k^*}{k}\right) = \frac{\vec{v}\cdot\hat{z}}{v_D}(1-k^*) \tag{50}$$

where $v_D = \frac{D_{interface}}{l_{interface}}$ is a "characteristic trapping velocity" which depends on the diffusion in the interface $D_{interface}$, and a length measure of the sharp-interface's effective width $l_{interface}$, which is not a predictable parameter but rather must be fit [23]. Eq. (50) is transcendental and can be approximated by expanding the logarithm. This expansion however is only good in the range of $\left|1-\frac{k^*}{k}\right| \leq 0$ which is acceptable for most previous models, however we wish to remove this limitation.

The determination of the concentration in the liquid at the interface is difficult in phase-field methods since the exact limits of the interface are blurred. Therefore we adopt the definition proposed by Ahmad *et al*:

$$k^* = \frac{c_i^{\alpha}}{max(c_i)} \tag{51}$$

which is technically only true if the peak occurs outside of the interfacial region. In examining the simulation results below, we see this is not always true, however in the absence of a discussion on interfacial adsorption this definition is adopted for our purposes.

We consider a binary solution with the parameters given in Table III and impose a range of interface velocities through Eq. (30), solving the resulting equations for the stationary state.

Figure 9 shows the results of the computer simulation with the sharp model predictions from Eq. (50) being

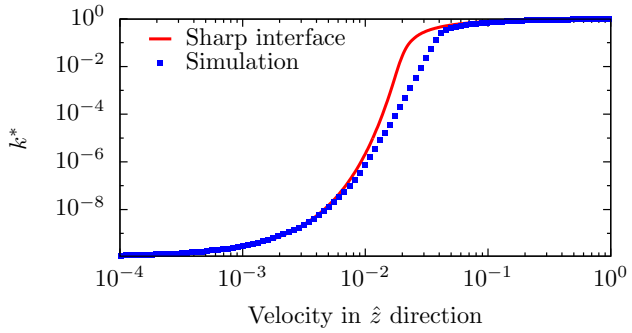

FIG. 9. Comparison of solute trapping predictions from simulation and sharp interface solution given in Eq. (50). System properties are given in Table III. $v_D = 1 \times 10^{-3}\,\mathrm{m\,s^{-1}}$

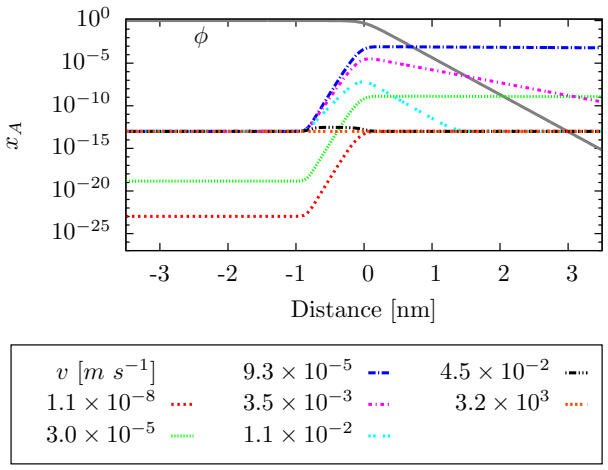

FIG. 10. Stationary state mole fraction profiles of species A as a function of interface velocity showing increasing solid concentration to the liquid far from the interface and the formation of the solute pile-up in the liquid phase. The phase-field variable is shown for reference, and velocities are as labelled in the key.

solved numerically using SciPy function *minimize_scalar*, which uses the Brent method [37]. The value $v_D = 0.001\,\mathrm{m\,s^{-1}}$ was selected manually matching the curves for slower velocities considering that for higher velocities, the peak in c_i moved into the interface, which may indicate interfacial adsorption and a poor determination k^*. It is gratifying to note however that $v_D = \frac{D_i}{10d}$. The factor of 10 may arise from the difference between the chosen interface width, d and the actual width of the calculated interface given by the solution 29b, which between $\phi = 1\%$ and 99% is approximately $10d$.

Figure 10 shows the simulated concentration profiles for velocities ranging from $1 \times 10^{-8}\,\mathrm{m\,s^{-1}}$ to $1 \times 10^{3}\,\mathrm{m\,s^{-1}}$ as indicted in the legend. The liquid phase is represented by phase α on the right side of the figure and, while the simulated domain extends 360 nm to the right, is cut off in order to resolve the details of the interface. While the liquid concentration far from the interface stays constant, the concentration in the solid rises to match it. Meanwhile the solute pile-up in the liquid phase increases several orders of magnitude at moderate velocities like $1 \times 10^{-6}\,\mathrm{m\,s^{-1}}$ before decreasing at high speeds. In examining the profile at $4.5 \times 10^{-2}\,\mathrm{m\,s^{-1}}$ one can see that the maximum concentration value has shifted towards the center of the interface.

E. Multicomponent interdiffusion with large partitioning and interstitial diffusion

An example of a quinary system at steady state, with zero bulk velocity is shown in Figure 11. The concentrations far from the interface are given in Table IV, with interface width, $\delta = 1\,\text{Å}$.

The results of the simulation are as one would expect, with the concentrations following the shape of the phase fraction p.

TABLE IV. Material properties for the quinary diffusion system.

Component	$c_i^\alpha\,[\mathrm{mol\,m^{-3}}]$	$c_i^\beta\,[\mathrm{mol\,m^{-3}}]$	k_i
A	38850	10^{-23}	3.885×10^{27}
B	10^{-23}	16650	6.006×10^{-28}
C	10^{-23}	11100	9.009×10^{-28}
D	$16650 - 2 \times 10^{-23}$	$27750 - 10^{-23}$	0.6
I	83250	10^{-23}	8.325×10^{27}

V. CONCLUSIONS

We have developed a phase-field model with multicomponent interdiffusion in which components can vary in excess of 23 orders of magnitude between phases. The model is formulated from a thermodynamic standpoint specially to give robust numerical solution behavior through the introduction of the pressure work mode and pressure driven diffusion. Material properties in the interface, notably the variation of the diffusion coefficient as a function of the phase, are derived from basic arguments.

Numerical robustness is achieved at the cost of performance, in terms of the number of unknowns to be solved for and the time steps required to achieve high accuracy. The logarithmic representation allows for tracking of a large range of concentration values without succumbing to round-off or truncation in lieu of extremely high computer precision.

Interfacial adsorption is not inherently present in the current model, in contrast with that of Wheeler *et al.*. Excellent reproduction of sharp interface analytical solutions for both binary diffusion couples and solute trap-

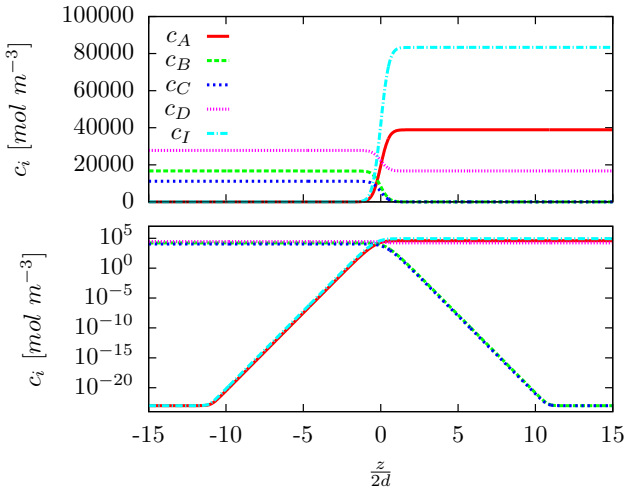

FIG. 11. Simulation results for a demonstrative quinary system, with 4 interdiffusing substitutional species and one interstitial, with linear and logarithmic concentrations above and below respectively. The concentration of normal lattice sites is $55\,500\,\mathrm{mol\,m^{-3}}$ with *insoluble* species set at $1\,\mathrm{atoms/m^3}$. Input parameters are given in Table IV.

ping with extremely large partition coefficients is demonstrated. Extensibility of the model is demonstrated by a quinary system.

ACKNOWLEDGMENTS

MJW wishes to acknowledge Dr. Shiyuan Gu for several helpful discussions of a mathematical nature. MJW was supported by the DOE-BES Computational Materials and Chemical Sciences Network (CMCSN) project on Computational Microstructure Science. DW and MJW were supported by UChicago Argonne, LLC, under contract No. DE-AC02-06CH11357.

[1] U. Grafe, B. Bo, J. Tiaden, and S. G. Fries, Scr. Mater. **42**, 1179 (2000).
[2] R. Qin, E. Wallach, and R. Thomson, J. of Cryst. Growth **279**, 163 (2005).
[3] R. Zhang, M. Li, and J. Allison, Comput. Mater. Sci. **47**, 832 (2010).
[4] R. Kobayashi, Physica D **63**, 410 (1993).
[5] O. Penrose and P. Fife, Physica D **43**, 44 (1990).
[6] A. A. Wheeler, W. J. Boettinger, and G. B. McFadden, Phys. Rev. A **45**, 7424 (1992).
[7] A. A. Wheeler, W. J. Boettinger, and G. B. McFadden, Phys. Rev. E **47**, 1893 (1993).
[8] A. A. Wheeler, G. B. McFadden, and W. J. Boettinger, Proc. R. Soc. London, Ser. A **452**, 495 (1996).
[9] S. G. Kim, W. T. Kim, and T. Suzuki, Phys. Rev. E **60**, 7186 (1999).
[10] S. G. Kim, W. T. Kim, and T. Suzuki, Phys. Rev. E **58**, 3316 (1998).
[11] J. Tiaden, B. Nestler, H. J. Diepers, and I. Steinbach, Physica D **115**, 73 (1998).
[12] I. Steinbach, Modell. Simul. Mater. Sci. Eng. **17**, 73001 (2009).
[13] S.-H. Kim, C.-Y. Joung, S.-C. Lee, and H.-S. Kim, Journal of Alloys and Compounds **441**, 23 (2007).
[14] J. Kim, Commun. Comput. Phys. **12**, 613 (2012).
[15] B. Nestler, H. Garcke, and B. Stinner, Phys. Rev. E **71**, 041609 (2005).
[16] J. E. Guyer, W. J. Boettinger, J. A. Warren, and G. B. McFadden, Phys. Rev. E **69**, 021603 (2004).
[17] J. E. Guyer, W. J. Boettinger, J. A. Warren, and G. B. McFadden, Phys. Rev. E **69**, 021604 (2004).
[18] G. Caginalp and W. Xie, Phys. Rev. E **48**, 1897 (1993).
[19] P. Cha, D. Yeon, and J. Yoon, Acta Materialia **49**, 3295 (2001).
[20] P.-R. Cha, D.-H. Yeon, and J.-K. Yoon, J. Cryst. Growth **274**, 281 (2005).
[21] M. Plapp, Phys. Rev. E **84**, 31601 (2011).
[22] M. J. Aziz, J. Appl. Phys. **53**, 1158 (1982).
[23] N. A. Ahmad, A. A. Wheeler, W. J. Boettinger, and G. B. McFadden, Phys. Rev. E **58**, 3436 (1998).
[24] D. L. Scharfetter and H. K. Gummel, Electron Devices, IEEE Transactions on **16**, 64 (1969).
[25] C. H. P. Lupis, *Chemical thermodynamics of materials* (North Holland, New York :, 1983) pp. xviii, 581 p. :.
[26] S. R. de Groot and P. Mazur, *Non-equilibrium thermodynamics* (Dover publications, New York, 1984).
[27] M. J. Welland, in *Comprehensive Nuclear Materials* (Elsevier Inc., 2012) 1st ed., Chap. Matter Tra, pp. 629–676.
[28] A. Logg, K.-A. Mardal, G. N. Wells, and Others, *Automated Solution of Differential Equations by the Finite Element Method* (Springer, 2012).
[29] A. Logg and G. N. Wells, ACM Transactions on Mathematical Software **37** (2010), 10.1145/1731022.1731030.
[30] A. Logg, G. N. Wells, and J. Hake, "DOLFIN: a C++/Python Finite Element Library," in *Automated Solution of Differential Equations by the Finite Element Method, Volume 84 of Lecture Notes in Computational Science and Engineering*, edited by A. Logg, K.-A. Mardal, and G. N. Wells (Springer, 2012) Chap. 10.
[31] A. Logg, K. B. \Olgaard, M. E. Rognes, and G. N. Wells, "FFC: the FEniCS Form Compiler," in *Automated Solution of Differential Equations by the Finite Element Method, Volume 84 of Lecture Notes in Computational Science and Engineering*, edited by A. Logg, K.-

A. Mardal, and G. N. Wells (Springer, 2012) Chap. 11.
[32] M. S. Alnæ s, A. Logg, K.-A. Mardal, O. Skavhaug, and H. P. Langtangen, Int. J. Comput. Sci. Eng. **4**, 231 (2009).
[33] K. E. Skare, *Gryphon - a Module for Time Integration of Partial Differential Equations in FEniCS*, Master of science in physics and mathematics, Norwegian University of Science and Technology (2012).
[34] A. Kvæ rnø, BIT Numerical Mathematics **44**, 489 (2004).
[35] A selection of code examples are available at www.mikewelland.com/publications/code.
[36] A. Karma, Phys. Rev. Lett. **87**, 1 (2001).
[37] E. Jones, T. Oliphant, P. Peterson, and Others, "SciPy: Open source scientific tools for Python,".